PCCP

Accepted Manuscript

ROYAL SOCIETY OF CHEMISTRY

www.rsc.org/pccp

Physical Chemistry Chemical Physics
CREATED USING THE RSC LaTeX PCCP ARTICLE TEMPLATE – SEE www.rsc.org/electronicfiles FOR DETAILS
ARTICLE TYPE www. rsc.org/xxxxxx | XXXXXXXX

Solvent Effects on the Photochemistry of 4-aminoimidazole-5-carbonitrile, a Prebiotically Plausible Precursor of Purines

Rafał Szabla,*[a] Judit E. Šponer,[a,b] Jiří Šponer[a,b], Andrzej L. Sobolewski,[c] and Robert W. Góra,*[d]

Received Xth XXXXXXXXXX 20XX, Accepted Xth XXXXXXXXX 20XX
First published on the web Xth XXXXXXXXXX 200X
DOI: 10.1039/b000000x

4-aminoimidazole-5-carbonitrile (AICN) was suggested as a prebiotically plausible precursor of purine nucleobases and nucleotides. Although it could be formed in a sequence of photoreactions, AICN is immune to further irradiation with UV-light. We present state-of-the-art multireference quantum-chemical calculations of potential-energy surface cuts and conical intersection optimizations to explain the molecular mechanisms underlying the photostability of this compound. We have identified the N–H bond stretching and ring-puckering mechanisms that should be responsible for the photochemistry of AICN in the gas phase. We have further considered the photochemistry of AICN–water clusters, while including up to six explicit water molecules. The calculations reveal charge transfer to solvent followed by formation of H_3O^+ cation both of which occur on the $^1\pi\sigma^*$ hypersurface. Interestingly, a second proton transfer to an adjacent water molecule leads to a $^1\pi\sigma^*/S_0$ conical intersection. We suggest that this electron-driven proton relay might be characteristic of low-lying $^1\pi\sigma^*$ states in chromophore–water clusters. Owing to its nature, this mechanism might also be responsible for the photostability of analogous organic molecules in bulk water.

1 Introduction

One of the most significant features of life is its remarkable biochemical unity. In this sense, all the diverse living organisms are composed of the same building blocks on the molecular level. The rather limited group of these biologically relevant molecules suggests a severe selection of their prebiotic precursors. Such a selection was probably driven by inclement environmental conditions of the Archean age. Thus, considering our knowledge about the evolution of environmental conditions on our planet, several scenarios have been proposed for the prebiotic synthesis of the components of the first informational polymers.[1–4]

Due to lack of the ozone layer in the atmosphere[5] and higher activity of the Sun in the ultraviolet range,[6,7] the amount of UV-B and UV-C reaching the surface of early Earth was much larger than nowadays. In the past twenty years, several research groups identified a number of relaxation mechanisms that protect nucleobases and peptides from the destructive effects of UV irradiation.[8–14] These findings support the hypothesis that UV light was one of the most important selection factors influencing abiogenesis. This also implies that the most significant intermediates on the prebiotic routes to nucleotides might have been photostable as well.

Over the past 50 years a lot of effort was put into finding an efficient synthesis of RNA building blocks under prebiotically plausible conditions. The most recent studies in this field report on the formation of pyrimidine nucleotides via a small aromatic compound—2-aminooxazole.[3,15] Persistent UV irradiation seems to play a key role in this reaction sequence, as it purifies the product mixture from biologically irrelevant stereoisomers of cytidine and uridine. In one of our recent works we studied photostability of 2-aminooxazole,[16] since Sutherland's scenario presumes its accumulation over longer periods of time.[17] Our results reveal that, indeed, such effective radiationless deactivation mechanisms of 2-aminooxazole exist.

On the other hand, one of the most plausible routes to purine nucleobases and nucleotides consists of oligomerization of hydrogen cyanide to diaminomaleonitrile (HCN tetramer) and its subsequent photoisomerisation that leads to a direct purine precursor—4-aminoimidazole-5-carbonitrile (AICN).[4,18–23] The formation of purines via AICN was studied under various conditions and it was confirmed that this prebiotic molecule can be also synthesized in formamide solutions and ices.[24,25] AICN is particularly interesting since it

† Electronic Supplementary Information (ESI) available: including plots of the electric dipole moment vectors for relevant states and Cartesian coordinates of the selected stationary point structures. See DOI: 10.1039/b000000x/

[a] *Institute of Biophysics, Academy of Sciences of the Czech Republic, Královopolská 135, 61265, Brno (Czech Republic); E-mail: rafal.szabla@gmail.com*
[b] *CEITEC–Central European Institute of Technology, Masaryk University, Campus Bohunice, Kamenice 5, CZ-62500 Brno, Czech Republic*
[c] *Institute of Physics, Polish Academy of Sciences, Al. Lotników 32/46, PL-02668 Warsaw, Poland*
[d] *Theoretical Chemistry Group, Institute of Physical and Theoretical Chemistry, Wrocław University of Technology, Wybrzeże Wyspiańskiego 27, 50-370 Wrocław, Poland. Fax: 48 71 320 3364; Tel: 48 71 320 4076; E-mail: robert.gora@pwr.edu.pl*

is immune to further irradiation with UV-light.[19] The mechanisms of its photochemical formation were recently thoroughly described.[26,27] Nevertheless, the mechanisms underlying the photostability of this compound have not been addressed yet. Thus, in this article we report multireference quantum-chemical calculations of the potential energy surface cuts and conical intersections that elucidate the non-radiative relaxation of UV-excited AICN molecule.

The mechanisms of photostability of several aromatic compounds similar to AICN were studied in detail by means of high-level quantum-chemical calculations and ultrafast time-resolved spectroscopic techniques.[16,28–40] According to these results, the ring-puckering and N–H bond stretching relaxation mechanisms reported for nucleobases, pyrrole, imidazole and 2-aminooxazole might be also important in the gas phase photochemistry of AICN. However, studies that address the solvent effects on the photostability of such systems are still scarce.[41] Therefore, in this article we also consider the influence of an environment by incorporating implicit solvent model as well as explicit water molecules. In particular, we discuss charge transfer to solvent (CTTS) processes and the trends which can be observed in the course of AICN microsolvation by water molecules.

2 Computational Methods

The ground-state equilibrium geometries of both AICN tautomers were optimized assuming C_s point-group symmetry or without any constraints (C_1), using the MP2/aug-cc-pVTZ method. These geometries were used in further calculations of vertical excitation energies. For comparison, we have also optimized the ground-state geometries at the B3LYP/6-311++G(2d,2p) level, including the solvent screening effects exerted by bulk water. For that purpose, we employed the conductor-like polarizable continuum model (C-PCM) including electrostatic, dispersion, exchange-repulsion and cavitation contributions as implemented in the GAUSSIAN 09 package.[42–45] Thermodynamic properties of the considered AICN tautomers were estimated assuming the rigid rotor and harmonic oscillator approximations.

Vertical excitation energies (see Tab. 1) were calculated using the state-specific CASPT2 energies computed based on the state-averaged CASSCF reference wave functions (SS-CASPT2//SA-CASSCF/aug-cc-pVDZ) of C_s symmetry, and at the CC2/aug-cc-pVTZ level, considering both C_s and C_1 symmetries. In the case of A' states of 1H-AICN the active space was constructed from four occupied π orbitals and four unoccupied π^* orbitals, thus comprising 8 electrons in 8 orbitals. The active space assumed in the case of A'' states of 1H-AICN was composed of two occupied π orbitals, three unoccupied σ^* orbitals, and one unoccupied π^* orbital, thus correlating 4 electrons in 6 orbitals. In the case of A' states of 3H-AICN the CAS consisted of four occupied π orbitals and three unoccupied π^* orbitals, that is 8 electrons in 7 orbitals. The active space used in the case of A'' states of 3H-AICN contained three occupied π orbitals and two unoccupied σ^* orbitals, thus correlating 6 electrons in 5 orbitals. These active spaces were carefully chosen on the basis of natural orbital occupations of the respective tautomers and symmetries. Nonequilibrium solvent screening effects on the vertical excitation energies (exerted by bulk water) were calculated using the C-PCM model.

The one-dimensional potential-energy profiles were obtained at the SS-CASPT2//SA-CASSCF/aug-cc-pVDZ levels described above. These profiles were constructed by calculating single-point energies along the N–H bond stretch coordinate for the MP2 optimized ground-state equilibrium geometries, assuming C_s symmetry. We performed rigid scans, since hydrogen-driven processes are usually much faster than other molecular motions, and within the period of an N–H bond stretching vibration the remaining coordinates should not change significantly.

The minima on the S_1/S_0 crossing seam (i.e. minimum-energy conical intersections) were optimized at the multireference configuration interaction level (MR-CISD) with the SA2-CASSCF(2,2)/cc-pVDZ reference wave function (the SA2 acronym indicates that the densities of the two states of interest were averaged). Thus, only one highest-lying π orbital and the lowest-lying σ^* (or π^* in the case of the *ring-puckered* CI) orbital were included in the active space. The corresponding potential energy profiles were obtained by linear interpolations in Pulay's internal coordinates (LIIC) between the Frank-Condon region and the minima on the crossing seams. The single-point energies on the LIIC paths were also calculated at the MR-CISD level and were adjusted with the Davidson type size-extensivity correction (MR-CISD+Q).

The optimizations of the $\pi\sigma^*$ equilibrium geometries of the AICN–water clusters and the relaxed potential-energy scans concerning the electron-driven double-proton transfer mechanism were performed at the ADC(2)/aug-cc-pVDZ level. The ADC(2) method provides description of electronically excited states with comparable quality as the MP2 level does for the electronic ground state.[46] The respective ground-state single-point energies were computed at the MP2/aug-cc-pVDZ level.

The CC2 vertical excitation energies as well as the MP2 and ADC(2) geometry optimizations were performed using the TURBOMOLE 6.3 package,[47–49] whereas the CASPT2 excitation energies were computed with the MOLCAS 7.6 package.[50,51] All the remaining calculations reported in this work were performed with the COLUMBUS 7.0 program package.[52–56]

3 Results and Discussion

Ground-state geometries The ground state geometries of AICN tautomers were optimized at the MP2 and B3LYP levels. We have considered two tautomers which differ in the position of the *(N)*-hydrogen atom in the imidazole ring. According to the respective position of the hydrogen atom we shall refer to these as either 1H-AICN or 3H-AICN (cf. Fig. 1). Both tautomers are nearly isoenergetic as the free energy difference between them, calculated at the B3LYP level in the C-PCM model of water solvent, amounts to 0.07 kcal/mol (3H-AICN being slightly more stable). Thus, both of the tautomers are predicted to be co-existing in water solution.

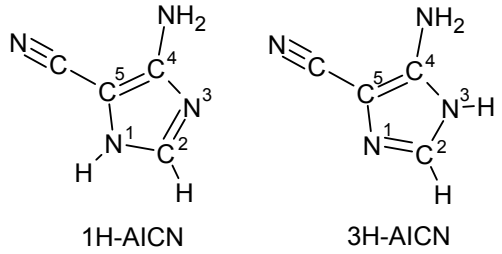

Fig. 1 Schematic drawing showing the two AICN tautomers considered in this study and the numbering of relevant atoms.

Vertical excitation energies The CC2 vertical excitation energies of both AICN tautomers calculated without any symmetry constraints are presented in Tab. 1.

The lowest-lying excited singlet state of AICN is a $^1\pi\sigma^*_{NH}$ state, which is repulsive with respect to N–H bond stretch. This is true for both of the considered tautomers and the respective vertical excitation energies are comparable as well (about 5.2 eV). In the case of 1H-AICN, the diffuse σ^* molecular orbital is localized around the hydrogen atom bonded to the N1 nitrogen atom in the aromatic ring (see Fig. 1 for atom numbering). The $^1\pi\sigma^*_{NH}$ state of 3H-AICN is repulsive with respect to to the N3–H bond and the nearby N–H bond of the amino group. That is, the respective σ^* molecular orbital spans the space around these two hydrogen atoms. This suggests a possible bifurcation of the N–H bond stretching relaxation mechanism, whenever the $^1\pi\sigma^*_{NH}$ state is reached after photoexcitation of 3H-AICN. It is worth to note that the electronic states described above resemble the S_1 states of pyrrole and 2-aminooxazole.[16,38] All these states can be classified as Rydberg-like excitations. The photochemistry of 3H-AICN is likely to be dominated by the repulsive $^1\pi\sigma^*_{NH}$ state due to sizable energy difference between this and higher-lying excited singlet states (about 0.6 eV).

The excitation energies to the optically bright states depend on the tautomer. In 1H-AICN, the $\pi\pi^*$ transition having the largest oscillator strength is the one to the S_2 state, which lies only 0.1 eV above the S_1 state (at the CC2 level). This small energy difference could allow these two states to interchange frequently. As a result, the ring puckering relaxation mechanism that occurs on the $\pi\pi^*$ hypersurface might significantly contribute to the photochemistry of this molecule. The two optically accessible states identified in 3H-AICN are of $\pi\pi^*$ character as well and have been classified as S_3 and S_4 states. However, 3H-AICN requires considerably higher energy ultraviolet radiation to populate one of these two states (about 6.00 eV). Although the wavelengths necessary to excite each of the AICN tautomers differ by more than 30 nm, in both cases these lie within the UV-C spectral range.

Table 1 Vertical excitation energies (in eV) of both AICN tautomers, computed assuming C_1 and C_s minimum energy structures

State / Transition		E_{exc}/[eV]	f_{osc}	λ/[nm]
1H-AICN (C_1); CC2/aug-cc-pVTZ				
S_1	$\pi\sigma^*$	5.13	$1.53\cdot10^{-2}$	241.7
S_2	$\pi\pi^*$	5.23	0.196	237.1
S_3	$\pi\sigma^*$	5.42	$1.09\cdot10^{-2}$	228.8
S_4	$\pi\sigma^*$	5.91	$6.70\cdot10^{-4}$	209.8
S_5	$\pi\pi^*$	6.10	$7.97\cdot10^{-2}$	203.3
1H-AICN (C_S); CASTP2//CASSCF/aug-cc-pVDZ				
(2-A')	$\pi\pi^*$	5.22 (4.98)[a]	0.151	237.5 (249.0)[a]
(1-A'')	$\pi\sigma^*$	5.14 (5.14)[a]	-	241.2 (241.2)[a]
3H-AICN (C_1); CC2/aug-cc-pVTZ				
S_1	$\pi\sigma^*$	5.24	$8.12\cdot10^{-3}$	236.6
S_2	$\pi\sigma^*$	5.84	$7.78\cdot10^{-3}$	212.3
S_3	$\pi\pi^*$	5.99	0.126	207.0
S_4	$\pi\pi^*$	6.13	0.135	202.3
S_5	$\pi\sigma^*$	6.47	$5.70\cdot10^{-3}$	190.6
3H-AICN (C_S); CASTP2//CASSCF/aug-cc-pVDZ				
(2-A')	$\pi\pi^*$	5.93 (5.65)[a]	0.118	209.1 (219.4)[a]
(1-A'')	$\pi\sigma^*$	4.43 (5.34)[a]	-	279.9 (253.6)[a]

[a] Energies calculated in the presence of the C-PCM model of bulk water.

N–H bond stretching mechanisms The N–H bond stretching mechanism was recognized as one of the primary radiationless deactivation mechanism in a variety of systems in the gas phase (e.g. pyrrole, indole, phenol, 2-aminooxazole and imidazole).[16,31–38,57] Since, there are three of such bonds in AICN, we have considered all of them in each of the tautomers. The respective potential-energy profiles computed at the CASPT2//SA-CASSCF level are shown in Fig. 2. These calculations were performed in the gas phase assuming C_s symmetry and only the three relevant states are shown for clar-

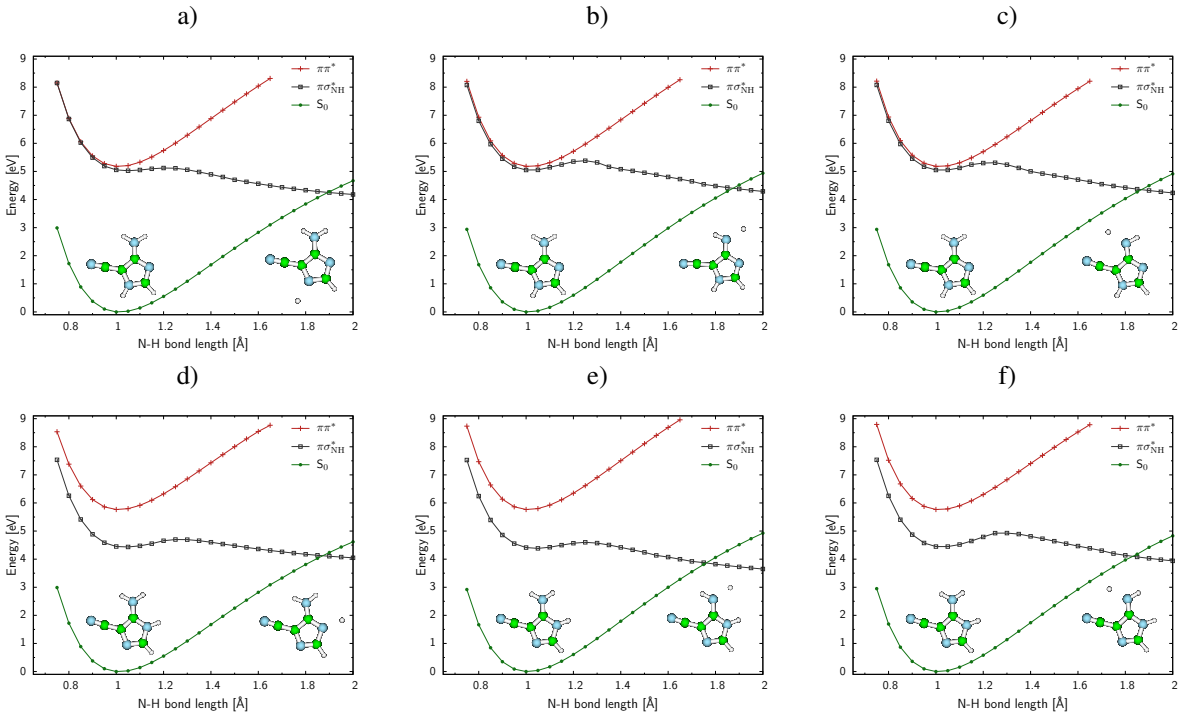

Fig. 2 Rigid scans along different N–H bonds' stretches of both considered AICN tautomers performed at CASPT2//CASSCF level assuming C_s symmetry. The optimized conical-intersection geometries are shown on the right-hand side of each graph. Color coding: C – green, N – blue, H – white.

ity.

Cleavage of any of the N–H bonds in AICN leads to an S_1/S_0 conical intersection at the R_{N-H} distances of approximately 1.80–1.90 Å. Each of the potential-energy curves reveals a shallow minimum in the Frank–Condon region of the $^1\pi\sigma^*_{NH}$ states. The emerging double-well shape of the $^1\pi\sigma^*$ potential-energy (PE) cross-sections is a common feature of Rydberg-like excitations.[58] In each case a rather insignificant energetic barrier separates the Frank–Condon region and the conical intersection with the electronic ground state. Nonetheless, despite all the similarities between these N–H bond stretching mechanisms, there are some subtle differences which provide valuable information regarding the importance of these relaxation processes for UV-excited AICN molecule.

For 1H-AICN, stretching of the N1–H bond is an almost barrierless process (see Fig. 2a). Elongation of the other two N–H bonds of the amino group is restricted by a slightly higher energetic barrier (Fig. 2b and 2c). Although this barrier is still quite small (0.2–0.3 eV), it might reduce the contribution of the amino N–H bond stretches to the deactivation of 1H-AICN. Furthermore, the repulsive character of the lowest-lying $^1\pi\sigma^*_{NH}$ state is associated with the N1–H bond. Thus, for most of the nuclear configurations in the Frank–Condon region the cleavage of the N1–H bond might be the primary deactivation process induced by $^1\pi\sigma^*$ states. Analysis of the wave function reveals also that an increase of the amino N–H distances over 1.3 Å leads to the change of excitation character of the S_1 state. Although the S_1 state can still be described as a $^1\pi\sigma^*_{NH}$ excitation, the respective σ^* molecular orbital is exchanged and at larger distances it spans the space near the amino group.

Similar conclusions can be drawn in the case of 3H-AICN. However, as it was mentioned before, the lowest-lying $^1\pi\sigma^*_{NH}$ state is repulsive with respect to the N3–H bond and the nearest N–H bond of the amino group (Fig. 2d and 2e). Accordingly, the PE curves that correspond to the stretching of these two bonds have very similar shapes and almost negligible energetic barriers. This observation confirms the likely bifurcation of the N–H bond stretching relaxation mechanism in 3H-AICN. Stretching of the other amino N–H bond, that points in direction of the cyano group, encounters a significant energy barrier of almost 0.5 eV (Fig. 2f). Cleavage of this particular bond leads to a similar change of the excitation character as the one found for the amino group of 1H-AICN.

The geometries of all the $^1\pi\sigma^*_{NH}/S_0$ conical intersections discussed in this section were optimized at the MR-CISD level. These structures are presented on the right-hand side

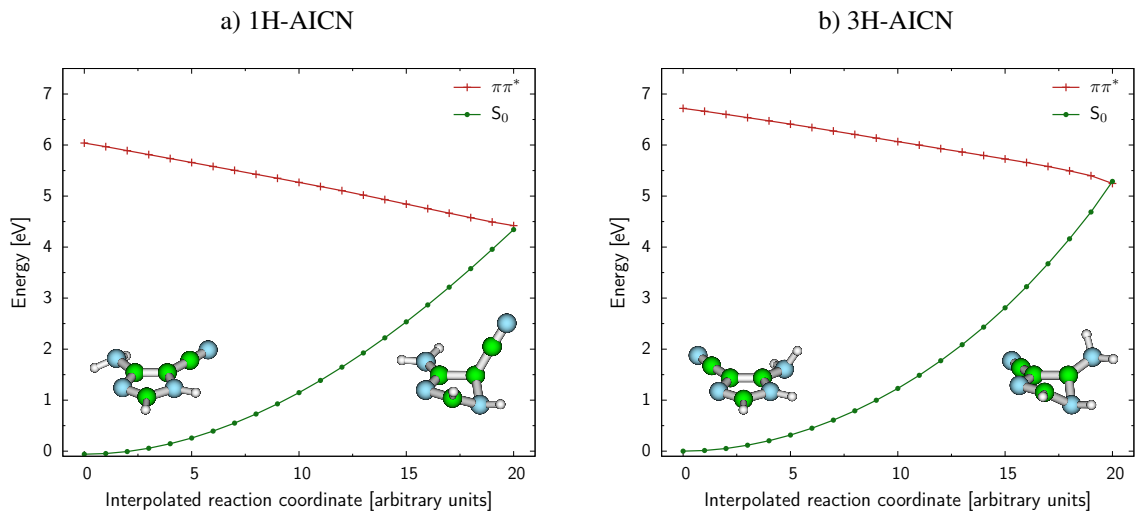

Fig. 3 LIICs between the ring-puckered conical intersections (optimized at the MR-CISD level) and the Franck–Condon regions of both considered AICN tautomers. Only the two relevant states are shown for clarity. The energies shown on the PE curves were calculated at the MR-CISD+Q level. Color coding: C – green, N – blue, H – white.

of each of the graphs in Fig. 2. The respective R_{N-H} distances of approximately 1.70–1.80 Å are in good agreement with the PE scans. In each case the energy-difference gradient vector **g** is dominated by the N–H bond stretching motion, while the non-adiabatic coupling vector **h** corresponds primarily to the out-of-plane tilting of the cleaved hydrogen atom. The Cartesian coordinates of the optimized geometries can be found in the Electronic Supplementary Information to this article.

Ring-puckering mechanisms Yet another non-radiative deactivation mechanism, which has already been described for analogous aromatic systems is the ring-puckering (see Fig. 3a and 3b). Such processes usually occur on the $^1\pi\pi^*$ hypersurfaces. It was shown that $^1\pi\pi^*$ states can be significantly stabilized by twisting around the C=C or C=N double bonds. Thus, if the S_1 state is of $^1\pi\pi^*$ character for a certain nuclear configuration, the two double bonds in the aromatic five-membered ring have enough time to twist. This twisting motion might eventually lead to a ring-puckered $^1\pi\pi^*/S_0$ conical intersection. We have located such conical intersections for both of the considered tautomers of AICN at the MR-CISD level. In each of the cases the H-substituted nitrogen atom of the ring is tilted out of the plane of the imidazole ring. In this sense, both of the located conical intersections are remarkably similar to the ring-puckered conical intersection found in pyrrole.[33] Interestingly, these processes are also barrierless (see Fig. 3). Therefore, ring-puckering could be potentially a very efficient mechanism of AICN deactivation.

It should be noted that according to our MR-CISD calculations, the ring-puckered conical intersection is the lowest energy conical intersection in 1H-AICN. In contrast, ring-puckering of UV-excited 3H-AICN leads to a $^1\pi\pi^*/S_0$ conical intersection, that lies 0.4–0.6 eV higher in energy than the remaining $^1\pi\sigma^*_{NH}/S_0$ minimum energy crossings. These relative energetic comparisons, however, are not necessarily the decisive factors. What determines the majority of the photochemical events after UV-excitation is the character of the lowest-lying excited electronic state and also its separation from higher-lying states. This has been observed for instance in non-adiabatic molecular dynamics simulations of a similar compound that is pyrrole,[33] in which the lowest energy conical intersection was found to be responsible for only 3% of the photochemistry of pyrrole.

Solvent effects on the vertical excitation energies Some preliminary conclusions regarding the influence of environment on the relaxation mechanisms of organic molecules can be drawn on the basis of solvatochromic shifts of vertical excitation energies. Polar solvents can influence excitation energies by stabilizing or destabilizing certain electronic states. Consequently, quantum yields of different radiationless relaxation processes might be affected as well. This is particularly true, if the ordering of the lowest-lying excited states is interchanged in a polar solvent with respect to the ordering found in gas phase. Thus, our preliminary conclusions regarding the influence of non-equilibrium solvation effects exerted by bulk water are based on C-PCM calculations.

Our CASPT2//CASSCF data show that the optically bright $^1\pi\pi^*$ transitions are red-shifted in both of the considered tautomers of AICN. In contrast, the $^1\pi\sigma^*_{NH}$ state in 3H-AICN is blue-shifted while the excitation energy of this state in 1H-AICN remains unchanged (see Tab. 1). This leads to a de-

creased energetic gap between these two states in 3H-AICN, but the $^1\pi\sigma^*_{NH}$ state remains the lowest-lying excited singlet state. However, in the case of 1H-AICN, this energetic gap is already quite small in the gas phase and the ordering of the two states is interchanged in bulk water. Hence, the S_1 state in 3H-AICN might be of $^1\pi\pi^*$ character in the Franck–Condon region, owing to the interaction with polar solvents. This would also imply that the ring-puckering is the most efficient deactivation channel for 1H-AICN in bulk water.

Although one would expect $^1\pi\sigma^*$ states to be more stabilized in polar solvents than $^1\pi\pi^*$ excitations,[38] such an assumption is inconsistent with our findings. Even though the $^1\pi\sigma^*_{NH}$ states discussed above are significantly more polar than the electronic ground state or the $^1\pi\pi^*$ state, these are not stabilized and can be even blue shifted in bulk water. This rather counterintuitive result can be explained by comparing the orientation and magnitudes of the electric dipole moment vectors (μ) of the relevant electronic states of AICN (ploted in Fig. 1 and 2 in the ESI). The μ vectors of the ground state and the optically bright $^1\pi\pi^*$ state have comparable magnitudes and similar directions in the case of both tautomers. Thus, transition from one state to the other is accompanied by rather minor charge redistribution, which can be almost instantaneously compensated by polarization of the nearby water molecules. In consequence, the vertical excitation energy is only slightly red-shifted. On the other hand, the $^1\pi\sigma^*_{NH}$ state has considerably larger electric dipole moment than these two states and its direction is completely different than that of the ground state. Thus in this case, the instantaneous polarization of the solvent molecules is not sufficient to balance the change of electronic density distribution and in effect, the $^1\pi\sigma^*_{NH}$ state is destabilized due to a non-equilibrium solvation.

Photochemistry of AICN–water clusters In the previous sections we have suggested that hydrogen detachment might be the primary photochemical process in AICN. This process, however, is expected to be substantially modified in water solution, since solvent molecules are able to intercept the detached protons. Some aspects of explicit water solvation in the photochemistry of $^1\pi\sigma^*$ states were previously addressed in case of phenol, pyrrole and indole molecules.[38,59–62] Similar effects have also been discussed involving an even better hydrogen acceptor—ammonia.[59,63–65] However, the previous studies considered the chromophore-water clusters of rather limited size and the respective geometries were usually optimized assuming C_s symmetry constraints. A $^1\pi\sigma^*/S_0$ conical intersection was found only for the pyrrole-ammonia pair and thus far a similar radiationless deexcitation mechanisms have not been documented in the case of clusters with water (to the best of our knowledge). In this section we attempt to shed some light on these processes in the case of the studied molecule in order to supplement the previous findings and to outline a general relaxation mechanism of $^1\pi\sigma^*$ states in water.

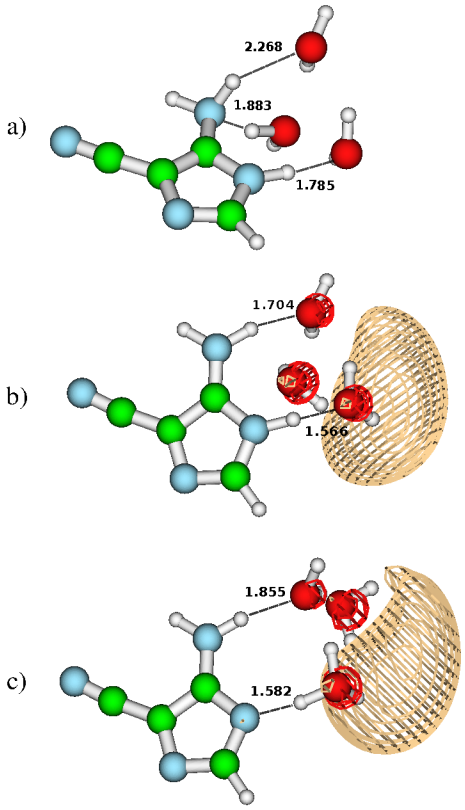

Fig. 4 Equilibrium geometries of 3H-AICN clusters with three water molecules: a) ground state, b) $^1\pi\sigma^*$ state, c) $^1\pi\sigma^*$ state - dissociated form including the H_3O^+ cation. The solvated electron is represented by the σ^* molecular orbital in b) and c).

The ground-state geometries of AICN-water clusters were optimized at the MP2 level, whereas the optimizations of the clusters in the S_1 state were performed at the ADC(2) level. We focus on the photochemistry of 3H-AICN–water clusters, since the S_1 state of 1H-AICN–water clusters is of $^1\pi\pi^*$ character. The optimizations of the S_1 state of 1H-AICN–water clusters lead to a structure, for which the ADC(2) approximation is no longer valid.

The basic geometrical differences between the optimized ground-state and $^1\pi\sigma^*$-state geometries are presented in Fig. 4. The figure shows the cluster of 3H-AICN with only three water molecules. However, the general conclusions are independent of the cluster size. The geometry of the AICN moiety in the minimum of the $^1\pi\sigma^*$ state is approximately planar as opposed to the ground-state geometry with pyramidalized amino group. The most remarkable difference is the complete redistribution of the hydrogen bonding network when the minimum on the $^1\pi\sigma^*$ surface is reached. The attractive interaction of the amino group lone electron pair and the hydro-

gen atom that belongs to the nearby water molecule is broken. Moreover, the two hydrogen bonds between the oxygen atoms of the two remaining water molecules and the hydrogen atoms of the AICN molecule are significantly shortened (by 0.56 and 0.22 Å respectively; compare Fig. 4a and 4b). This feature of the optimized $^1\pi\sigma^*$-state geometry of the cluster is a direct consequence of the CTTS process. In other words, the excited electron is ejected from the aromatic ring and charge separation occurs. The amount of electronic charge transfered to solvent at various stationary points on the S_1 surface amounts to about 1e according to the results of Mulliken population analysis. The plots of relevant difference-densities are available as supplementary information to this paper (cf. Fig. 3 of ESI). In larger clusters with five or six water molecules the corresponding electronic density is encapsulated by the solvent molecules and thus shielded from the positively charged chromophore. Interestingly, the two hydrogen bonds marked in Fig. 4b are getting shorter with every water molecule consecutively attached to the cluster (the distances are listed in Tab. 2).

We further investigated the possibility of an excited-state proton transfer from the positively charged 3H-AICN to the nearby water molecule. We thus cleaved the N3–H bond to arrive at another minimum of the AICN-water clusters on the $^1\pi\sigma^*$ hypersurface. This minimum was found for all the studied clusters and it consists of a AICN· and a H_3O· radicals. The energetic barrier observed for this process is lower than 0.10 eV for all the studied clusters and the position of the proton can be easily interchanged between the chromophore and the nearby water molecule. In the case of clusters composed of AICN and five water molecules (or more) the electron ejected to the σ^* orbital is, in fact, completely shielded from the H_3O^+ cation. Thus, for instance, the dissociated minimum on the $^1\pi\sigma^*$ hypersurface of the 3H-AICN cluster with five water molecules consists of AICN· radical, H_3O^+ cation and the electron in the σ^* orbital pre-solvated by four remaining water molecules (Fig. 5a).

It was observed for phenol-water clusters that energy of the dissociated minimum of the $^1\pi\sigma^*$ state is systematically lowered with an increasing number of water molecules.[59] We have observed the same trend for 3H-AICN-water clusters. In the case of the AICN cluster with one water molecule the dissociated minimum that involves the H_3O· radical, lies 0.09 eV above the non-dissociated form. Adding additional two water molecules slightly lowers the energy difference and the two minima are nearly isoenergetic when considering the cluster with four solvent molecules. In the case of clusters with five and six water molecules the dissociated forms are already energetically more stable (by 0.08 and 0.12 eV respectively; see Tab. 2) than the non-dissociated forms on the $^1\pi\sigma^*$ hypersurface. This implies that the formation of the H_3O^+ cations and hydrated electrons might be the primary process that occurs after the photoexcitation of 3H-AICN in water solution. It is worth to note that the formation of the hydronium cation does not lead to a conical intersection and this minimum of the $^1\pi\sigma^*$ state lies far over 1.0 eV above the ground state. Therefore, another photochemical process is necessary to enable the radiationless deactivation of the clusters to the electronic ground state.

Recently Zilberg *et. al* proposed a mechanism of non-radiative relaxation of the pyrrole–ammonia cluster through a two-body dissociation channel.[64] This mechanism might occur following the excited state proton transfer from pyrrole to ammonia. The respective conical intersection is reached after the dissociation of the pyrrolyl and NH_4· radical pair. We have found an analogous conical intersection due to the separation of AICN· and H_3O· radical pair. This conical intersection was optimized at the MR-CISD level, and it has a sloped topography similarly as in the case of the pyrrole–ammonia pair. The geometry at this conical intersection can be viewed in the ESI. Nevertheless, free migration of a H_3O^+ cation would be hindered in larger assemblies by strong interactions with neighboring water molecules. Therefore, this mechanism seems to be rather improbable in bulk water.

An alternative radiationless deactivation mechanism of AICN–water clusters might involve a second proton transfer from the H_3O^+ cation to the neighboring water molecule that interacts with the σ^* orbital. This process is much more plausible in bulk water and, thus, it is particularly interesting. We have considered such a possibility in the 3H-AICN cluster with five water molecules, since it is the smallest cluster having dissociated form which is a more favorable minimum on the $^1\pi\sigma^*$ hypersurface. The relaxed scan along the O–H bond of the H_3O^+ cation that points in the direction of the nearby H_2O molecule was performed at the ADC(2) level. In consequence, we have found a conical intersection at the R_{O-H} distance of 1.55 Å. Similarly as in the two-body dissociation process, the PE cross-section is ascending and the respective conical intersection has a sloped topography. This implies that the $^1\pi\sigma^*$ state of AICN–water clusters might be rather long-lived after the first proton transfer that forms the H_3O^+ cation. However, the energetic barrier that has to be overcome is low (approximately 0.3 eV) and this conical intersection might be still easily accessed in AICN–water clusters. Interestingly, this specific mechanism and the sloped topography of the respective conical intersection are reminiscent of the electron-driven proton transfer processes reported for Watson–Crick base pairs.[28,29]

Proton transfer in the excited $^1\pi\sigma^*$ state between the neighbouring water molecules encounters modest energetic barriers. The respective PE profiles are rather flat and a proton can be easily relayed to the neighborhood of the hydrated electron. However, in the electronic ground state, the movement of the proton is represented by dissociation to $AICN^-$ and

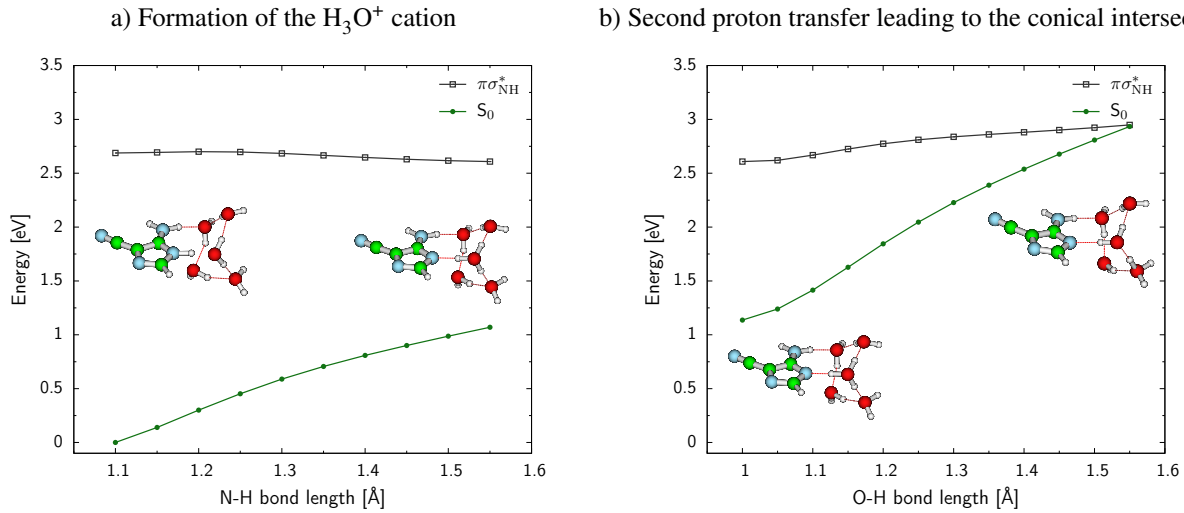

Fig. 5 Relaxed scans that represent the electron-driven double-proton transfer relaxation mechanism. The constrained optimizations in the S_1 state were performed at ADC(2) level of theory, whereas the respective ground-state energies were calculated using the MP2 method. Color coding: C – green, O – red, N – blue, H – white.

H_3O^+ ionic pair. The ground-state PE profile is strongly dependent on the distance that separates the ionic pair due to the Coulombic interaction of the charges localized on the $AICN^-$ and H_3O^+ molecules. In consequence, the S_1 and S_0 hypersurfaces cross for certain positions of the mobile proton in the cluster. Once the conical intersection is reached, the hydrated electron and subsequently the mobile proton may be returned to the AICN molecule, preserving the initial form of 3H-AICN molecule.

The mechanism of ground–state proton transfers from H_3O^+ cations to neighbouring water molecules was fully understood on the basis of quantum-chemical calculations and path integral molecular dynamics. The respective free–energy barrier was proved to be negligible ($\leq$ 0.15 kcal/mol).[66–68] The formation of the H_3O^+ cation is the initial step that occurs on the $^1\pi\sigma^*$ hypersurface of the studied AICN–water assemblies. The nature of the subsequent proton transfers to further water molecules will most likely be very similar to the aforementioned ground-state behavior of the hydrated excess proton in water. In this sense, the electron-driven proton relay might also be the primary mechanism of the photostability of 3H-AICN in bulk water.

4 Conclusions

In conclusion, we have performed ab-initio electronic structure and reaction-path calculations to elucidate the mechanisms of non-radiative relaxation of AICN. This molecule was proposed to be an important intermediate in the UV–induced formation of purine nucleobases and nucleotides.[4,18,19] Since AICN was found to be photostable during this prebiotically plausible synthesis,[19] the radiationless relaxation mechanisms of this compound are of particular interest for prebiotic chemistry.

In both of the considered AICN tautomers the lowest-lying excited singlet states are of $^1\pi\sigma^*$ character. These states are repulsive with respect to the N–H bond stretching. Rupture of each of the three N–H bonds in AICN leads to an S_1/S_0 conical intersection. Thus, all the mechanisms may contribute to radiationless deexcitation of the title compound in the gas phase. These conical intersections reveal many similarities to

Table 2 Selected properties of AICN–water clusters optimized in the S_1 state at the ADC(2)/auc-cc-pVDZ level

Cluster size[a]	ΔE^b_{deprot}	R(N3–H...OH_2)[c]	R($N_{am.}$–H...OH_2)[d]
3H-AICN–W_1	$9.21 \cdot 10^{-2}$	1.556	-
3H-AICN–W_2	$1.23 \cdot 10^{-1}$	1.568	1.668
3H-AICN–W_3	$7.15 \cdot 10^{-2}$	1.566	1.704
3H-AICN–W_4	$4.30 \cdot 10^{-3}$	1.508	1.681
3H-AICN–W_5	$-8.25 \cdot 10^{-2}$	1.460	1.679
3H-AICN–W_6	$-1.22 \cdot 10^{-1}$	1.438	1.657

[a] The subscript indicates the number of water molecules in the cluster.
[b] Energy difference calculated between the deprotonated and protonated minima of 3H-AICN on the S_1 hypersurface [eV].
[c] Hydrogen bond length between the N3–H hydrogen atom and the nearest water molecule [Å].
[d] Hydrogen bond length between the hydrogen atom of the amino group and the nearest water molecule [Å]. See also Fig. 4

the analogous photoinduced processes that occur in pyrrole, imidazole and 2-aminooxazole. Our results indicate that the N–H bond stretching mechanisms are likely to be the predominant deexcitation channels of the title compound in the gas phase. We have also investigated possible ring-puckering mechanisms driven by the simultaneous twisting of the double bonds of the aromatic imidazole ring. This relaxation channel occurs on the $^1\pi\pi^*$ hypersurface and the respective conical intersection with the electronic ground state can be reached in a barrierless manner. Therefore, ring-puckering might effectively compete with N–H bond cleavage mechanisms of both AICN tautomers.

According to our results, the optically bright $^1\pi\pi^*$ states of both of the considered AICN tautomers are red-shifted in bulk water. As a result the energetic gap between the $^1\pi\pi^*$ and $^1\pi\sigma^*_{NH}$ states of 3H-AICN is decreased in bulk water, whereas the ordering of these two states in 1H-AICN is interchanged. Consequently, the photodynamics of 1H-AICN in solution might be dominated by the ring-puckering mechanism. The $^1\pi\sigma^*$ states are not stabilized at all and may even be blue-shifted in bulk water. We explain this phenomenon on the basis of considerable differences between the magnitudes and directions of the ground-state and $^1\pi\sigma^*$-state electric dipole moments.

The inclusion of explicit water molecules is essential in order to better understand the influence of the environment on the photochemistry of 3H-AICN and similar molecules. In particular, we observe that once the $^1\pi\sigma^*_{NH}$ state is reached, an electron is transferred from the chromophore towards the explicit water molecules. This charge-transfer-to-solvent process that occurs in all the studied 3H-AICN–water clusters might further lead to the cleavage of N3–H bond. In consequence, a H_3O^+ cation is formed and the ejected electron is surrounded by the remaining water molecules. A rather low energetic barrier of this process (≤ 0.1 eV) indicates that the proton can be quickly interchanged between AICN and the neighbouring H_2O molecule. For the clusters that consist of 3H-AICN and five water molecules (or more), the dissociated minimum with the H_3O^+ cation is lower in energy than the non-dissociated form.

We have considered the possibility of yet another proton transfer event from the H_3O^+ cation to the H_2O molecule, which is adjacent to the solvated electron in the σ^* orbital. This process leads to a sloped $^1\pi\sigma^*/S_0$ conical intersection. Such an electron-driven proton relay might be a primary mechanism of radiationless deexcitation of low-lying $^1\pi\sigma^*$ states in chromophore–water clusters. Owing to its nature, this mechanism might also be responsible for the relaxation of analogous UV-excited organic molecules in bulk water. It is worth to note that to the best of our knowledge such a mechanism has not been reported before.

5 Abbreviations

AICN – 4-aminoimidazole-5-carbonitrile
CAS – complete active space
CTTS – charge transfer to solvent
LIIC – linear interpolation in internal coordinates
PE – potential-energy

6 Acknowledgments

This work was supported by the Grant Agency of the Czech Republic (grant No. 14-12010S) to J.E.S. and a statutory activity subsidy from the Polish Ministry of Science and Higher Education for the Faculty of Chemistry of Wrocław University of Technology to R.W.G. Financial support from the project "CEITEC–Central European Institute of Technology" (CZ.1.05/1.1.00/02.0068) from the European Regional Development Fund is gratefully acknowledged.

Part of the calculations was performed at the Wroclaw Center for Networking and Supercomputing (WCSS).

References

1 L. E. Orgel, *Critical Reviews in Biochemistry and Molecular Biology*, 2004, **39**, 99–123.
2 R. Saladino, G. Botta, S. Pino, G. Costanzo and E. Di Mauro, *Chem. Soc. Rev.*, 2012, **41**, 5526–5565.
3 M. W. Powner, B. Gerland and J. D. Sutherland, *Nature*, 2009, **459**, 239–242.
4 M. W. Powner, J. D. Sutherland and J. W. Szostak, *J. Am. Chem. Soc.*, 2010, **132**, 16677–16688.
5 J. F. Kasting, *Science*, 1993, **259**, 920–926.
6 C. S. Cockell, *J. Theor. Biol.*, 1998, **193**, 717–729.
7 A. P. Buccino, P. J. D. Mauas and G. A. Lemarchand, *Bioastronomy 2002: Life Among the Stars*, Astronomical Soc Pacific, San Francisco, 2004, pp. 97–100.
8 A. L. Sobolewski and W. Domcke, *Europhysics News*, 2006, **37**, 20–23.
9 M. Barbatti, A. J. A. Aquino, J. J. Szymczak, D. Nachtigallová, P. Hobza and H. Lischka, *Proc. Natl. Acad. Sci. U.S.A.*, 2010, 21453–21458.
10 K. Kleinermanns, D. Nachtigallová and M. S. de Vries, *Int. Rev. in Phys. Chem.*, 2013, **32**, 308–342.
11 M. S. de Vries and P. Hobza, *Annu. Rev. Phys. Chem.*, 2007, **58**, 585–612.
12 W. Domcke and A. L. Sobolewski, *Nat. Chem.*, 2013, **5**, 257–258.
13 M. Mališ, Y. Loquais, E. Gloaguen, H. S. Biswal, F. Piuzzi, B. Tardivel, V. Brenner, M. Broquier, C. Jouvet,

M. Mons, N. Došlić and I. Ljubić, *J. Am. Chem. Soc.*, 2012, **134**, 20340–20351.
14 C. Canuel, M. Mons, F. Piuzzi, B. Tardivel, I. Dimicoli and M. Elhanine, *J. Chem. Phys.*, 2005, **122**, 074316.
15 M. Powner, J. Sutherland and J. Szostak, *Synlett*, 2011, **2011**, 1956–1964.
16 R. Szabla, D. Tuna, R. W. Góra, J. Šponer, A. L. Sobolewski and W. Domcke, *J. Phys. Chem. Lett.*, 2013, **4**, 2785–2788.
17 J. W. Szostak, *Nature*, 2009, **459**, 171–172.
18 J. P. Ferris and L. E. Orgel, *J. Am. Chem. Soc.*, 1966, **88**, 1074–1074.
19 J. P. Ferris and J. E. Kuder, *J. Am. Chem. Soc.*, 1970, **92**, 2527–2533.
20 J. P. Ferris and R. W. Trimmer, *J. Org. Chem.*, 1976, **41**, 19–24.
21 J. P. Ferris, P. C. Joshi, E. H. Edelson and J. G. Lawless, *J. Mol. Evol.*, 1978, **11**, 293–311.
22 J. P. Ferris and E. H. Edelson, *J. Org. Chem.*, 1978, **43**, 3989–3995.
23 J. P. Ferris, R. S. Narang, T. A. Newton and V. R. Rao, *J. Org. Chem.*, 1979, **44**, 1273–1278.
24 M. Ferus, S. Civiš, A. Mládek, J. Šponer, L. Juha and J. E. Šponer, *J. Am. Chem. Soc.*, 2012, **134**, 20788–20796.
25 H. L. Barks, R. Buckley, G. A. Grieves, E. Di Mauro, N. V. Hud and T. M. Orlando, *ChemBioChem*, 2010, **11**, 1240–1243.
26 E. Boulanger, A. Anoop, D. Nachtigallova, W. Thiel and M. Barbatti, *Angew. Chem. Int. Ed.*, 2013, **125**, 8158–8161.
27 R. Szabla, R. W. Góra, J. Šponer and J. E. Šponer, *Chem. Eur. J.*, 2014, **20**, 2515–2521.
28 A. L. Sobolewski, W. Domcke and C. Hättig, *Proc. Natl. Acad. Sci. U.S.A.*, 2005, **102**, 17903–17906.
29 S. Perun, A. L. Sobolewski and W. Domcke, *J. Phys. Chem. A*, 2006, **110**, 9031–9038.
30 M. Barbatti, A. J. A. Aquino, J. J. Szymczak, D. Nachtigallová and H. Lischka, *Phys. Chem. Chem. Phys.*, 2011, **13**, 6145–6155.
31 M. Barbatti, M. Vazdar, A. J. A. Aquino, M. Eckert-Maksic and H. Lischka, *J. Chem. Phys.*, 2006, **125**, 164323.
32 H. Lippert, H.-H. Ritze, I. V. Hertel and W. Radloff, *ChemPhysChem*, 2004, **5**, 1423–1427.
33 M. Vazdar, M. Eckert-Maksić, M. Barbatti and H. Lischka, *Mol. Phys.*, 2009, **107**, 845–854.
34 M. Barbatti, J. Pittner, M. Pederzoli, U. Werner, R. Mitrić, V. Bonačić-Koutecký and H. Lischka, *Chem. Phys.*, 2010, **375**, 26–34.
35 A. L. Sobolewski and W. Domcke, *Chem. Phys.*, 2000, **259**, 181–191.
36 R. Crespo-Otero, M. Barbatti, H. Yu, N. L. Evans and S. Ullrich, *ChemPhysChem*, 2011, **12**, 3365–3375.
37 M. Barbatti, H. Lischka, S. Salzmann and C. M. Marian, *J. Chem. Phys.*, 2009, **130**, 034305.
38 A. L. Sobolewski, W. Domcke, C. Dedonder-Lardeux and C. Jouvet, *Phys. Chem. Chem. Phys.*, 2002, **4**, 1093–1100.
39 G. M. Roberts, C. A. Williams, M. J. Paterson, S. Ullrich and V. G. Stavros, *Chem. Sci.*, 2012, **3**, 1192–1199.
40 G. M. Roberts and V. G. Stavros, *Chem. Sci.*, 2014, **5**, 1698–1722.
41 T. Gustavsson, R. Improta and D. Markovitsi, *J. Phys. Chem. Lett.*, 2010, **1**, 2025–2030.
42 V. Barone and M. Cossi, *J. Phys. Chem. A*, 1998, **102**, 1995–2001.
43 G. Scalmani and M. J. Frisch, *J. Chem. Phys.*, 2010, **132**, 114110–114110–15.
44 J. Tomasi, B. Mennucci and R. Cammi, *Chem. Rev.*, 2005, **105**, 2999–3094.
45 M. J. Frisch, G. W. Trucks, H. B. Schlegel, G. E. Scuseria, M. A. Robb, J. R. Cheeseman, G. Scalmani, V. Barone, B. Mennucci, G. A. Petersson, H. Nakatsuji, M. Caricato, X. Li, H. P. Hratchian, A. F. Izmaylov, J. Bloino, G. Zheng, J. L. Sonnenberg, M. Hada, M. Ehara, K. Toyota, R. Fukuda, J. Hasegawa, M. Ishida, T. Nakajima, Y. Honda, O. Kitao, H. Nakai, T. Vreven, J. Montgomery, J. E. Peralta, F. Ogliaro, M. Bearpark, J. J. Heyd, E. Brothers, K. N. Kudin, V. N. Staroverov, R. Kobayashi, J. Normand, K. Raghavachari, A. Rendell, J. C. Burant, S. S. Iyengar, J. Tomasi, M. Cossi, N. Rega, J. M. Millam, M. Klene, J. E. Knox, J. B. Cross, V. Bakken, C. Adamo, J. Jaramillo, R. Gomperts, R. E. Stratmann, O. Yazyev, A. J. Austin, R. Cammi, C. Pomelli, J. W. Ochterski, R. L. Martin, K. Morokuma, V. G. Zakrzewski, G. A. Voth, P. Salvador, J. J. Dannenberg, S. Dapprich, A. D. Daniels, O. Farkas, J. B. Foresman, J. V. Ortiz, J. Cioslowski and D. J. Fox, *Gaussian 09, revision C.01*, 2009, Gaussian Inc. Wallingford CT.
46 J. Schirmer, *Phys. Rev. A*, 1982, **26**, 2395–2416.
47 C. Hättig and F. Weigend, *J. Chem. Phys.*, 2000, **113**, 5154–5161.
48 F. Weigend and M. Häser, *Theor. Chem. Acta.*, 1997, **97**, 331–340.
49 *TURBOMOLE v6.3 2011, a development of University of Karlsruhe and Forschungszentrum Karlsruhe GmbH, 1989-2007, TURBOMOLE GmbH, since 2007*, 2011, http://www.turbomole.com.
50 G. Karlström, R. Lindh, P.-A. Malmqvist, B. O. Roos, U. Ryde, V. Veryazov, P.-O. Widmark, M. Cossi, B. Schimmelpfennig, P. Neogrady and L. Seijo, *Comp. Mat. Sci.*, 2003, **28**, 222–239.

51 F. Aquilante, L. De Vico, N. Ferre, G. Ghigo, P.-A. Malmqvist, P. Neogrady, T. B. Pedersen, M. Pitonak, M. Reiher, B. O. Roos, L. Serrano-Andres, M. Urban, V. Veryazov and R. Lindh, *J. Comput. Chem.*, 2010, **31**, 224–247.

52 H. Lischka, R. Shepard, F. B. Brown and I. Shavitt, *Int. J. Quantum Chem. Symp.*, 1981, **15**, 91–100.

53 R. Shepard, I. Shavitt, R. Pitzer, D. Comeau, M. Pepper, H. Lischka, P. Szalay, R. Ahlrichs, F. Brown and J. Zhao, *Int. J. Quantum Chem. Symp.*, 1988, **22**, 149–165.

54 H. Lischka, R. Shepard, R. M. Pitzer, I. Shavitt, M. Dallos, T. Müller, P. G. Szalay, M. Seth, G. S. Kedziora, S. Yabushita and Z. Zhang, *Phys. Chem. Chem. Phys.*, 2001, **3**, 664–673.

55 H. Lischka, T. Müller, P. G. Szalay, I. Shavitt, R. M. Pitzer and R. Shepard, *Wiley Interdiscip. Rev. Comput. Mol. Sci*, 2011, **1**, 191–199.

56 H. Lischka, R. Shepard, I. Shavitt, R. M. Pitzer, M. Dallos, T. Müller, P. G. Szalay, F. B. Brown, R. Ahlrichs, H. J. Böhm, A. Chang, D. C. Comeau, R. Gdanitz, H. Dachsel, C. Ehrhardt, M. Ernzerhof, P. Höchtl, S. Irle, G. Kedziora, T. Kovar, V. Parasuk, M. J. M. Pepper, P. Scharf, H. Schiffer, M. Schindler, M. Schüler, M. Seth, E. A. Stahlberg, J.-G. Zhao, S. Yabushita, Z. Zhang, M. Barbatti, S. Matsika, M. Schuurmann, D. R. Yarkony, S. R. Brozell, E. V. Beck, J.-P. Blaudeau, M. Ruckenbauer, B. Sellner, F. Plasser and J. J. Szymczak, *COLUMBUS, relase 7.0 2012, an ab initio electronic structure program*, 2012, http://www.univie.ac.at/columbus.

57 A. L. Sobolewski and W. Domcke, *Chem. Phys. Lett.*, 1999, **315**, 293–298.

58 M. N. R. Ashfold, G. A. King, D. Murdock, M. G. D. Nix, T. A. A. Oliver and A. G. Sage, *Phys. Chem. Chem. Phys.*, 2010, **12**, 1218–1238.

59 A. L. Sobolewski and W. Domcke, *J. Phys. Chem. A*, 2001, **105**, 9275–9283.

60 A. L. Sobolewski and W. Domcke, *Chem. Phys. Lett.*, 2000, **321**, 479–484.

61 A. L. Sobolewski and W. Domcke, *Chem. Phys. Lett.*, 2000, **329**, 130–137.

62 A. Peralta Conde, V. Ovejas, R. Montero, F. Castaño and A. Longarte, *Chem. Phys. Lett.*, 2012, **530**, 25–30.

63 O. David, C. Dedonder-Lardeux, C. Jouvet, H. Kang, S. Martrenchard, T. Ebata and A. L. Sobolewski, *J. Chem. Phys.*, 2004, **120**, 10101–10110.

64 S. Zilberg, A. Kahan and Y. Haas, *Phys. Chem. Chem. Phys.*, 2012, **14**, 8836–8841.

65 O. David, C. Dedonder-Lardeux and C. Jouvet, *Int. Rev. Phys. Chem.*, 2002, **21**, 499–523.

66 M. Tuckerman, K. Laasonen, M. Sprik and M. Parrinello, *J. Phys. Chem.*, 1995, **99**, 5749–5752.

67 K. Ando and J. T. Hynes, *J. Phys. Chem. B*, 1997, **101**, 10464–10478.

68 D. Marx, M. E. Tuckerman, J. Hutter and M. Parrinello, *Nature*, 1999, **397**, 601–604.

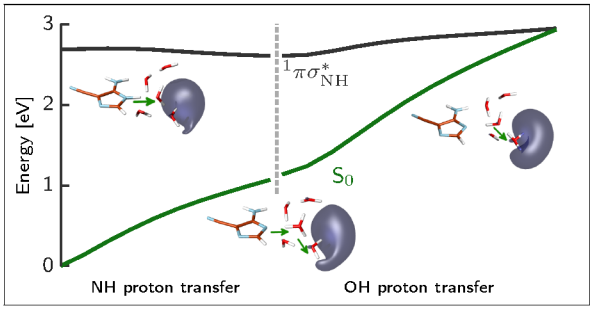

Ab initio studies elucidate the molecular mechanisms underlying photostability of a prebiotically plausible precursor of purine nucleotides, indicating importance of charge-transfer-to-solvent processes.